

MOL#43042

**Wide turn diversity in protein transmembrane helices**  
Implications for G-protein coupled receptor and other polytopic  
membrane protein structure and function

*R. Peter Riek, Angela A. Finch, Gillian E. Begg and Robert M. Graham*

*Computational and Structural Biology Division (R.P.R.) and Molecular Cardiology Program  
(A.F., G.B., R.M.G.) Victor Chang Cardiac Research Institute, Darlinghurst, 2010, New  
South Wales, Australia*

MOL#43042

*Running title:* Wide turn diversity in transmembrane helices

*Corresponding author:* Dr. Robert M. Graham

384 Victoria Street,

Darlinghurst, NSW 2010

Australia

Tel: 612-9295-8515 Fax: 612-9295-8501

e-mail – [b.graham@victorchang.edu.au](mailto:b.graham@victorchang.edu.au)

Number of pages: 30

Number of Tables: 4

Number of Supplemental Data Tables: 1

Number of Figures: 8

Number of Supplemental Data Figures: 4

Number of References: 37

Word count:

*Abstract:* 202

*Introduction:* 543

*Results and Discussion:* 3272

Abbreviations: H-bond, hydrogen bond; BCCO, bovine cytochrome C oxidase.

## **Abstract**

Previously we showed that perturbations of protein transmembrane helices are manifested as one

MOL#43042

of three types of non-canonical structures (wide turns, tight turns and kinks), which, as compared to  $\alpha$ -helices, are evident by distinctive  $C\alpha_i \rightarrow C\alpha_x$  distances. Here we report the analysis of over 3,000 transmembrane helices in 244 crystal structures from which we identified 70 wide turns (29 proline- and 41 non-proline-induced). Based on differences in the  $C\alpha_i \rightarrow C\alpha_{i-4}$  and  $C\alpha_i \rightarrow C\alpha_{i-5}$  profiles, we show that wide turns can be subclassified into three distinct subclasses ( $W_1$ ,  $W_2$  and  $W_3$ ) that differ with regards to the number and position of backbone  $i \rightarrow i-5$  H-bonds formed N-terminal to the perturbing or signature proline or non-proline residue. Although wide turns generally produce changes in helical direction of  $20^\circ$ - $30^\circ$  and a lateral shift in the helical axis, some of the  $W_3$  subclass are associated with changes of  $<5^\circ$ . We also show that the distinct architectural features of wide turns allow the carbonyl bond of the  $i-4$ th residue, which is located on the widened loop of a wide turn, to be directed away from the helical axis. This provides regions of flexibility within helical regions allowing, for example, unique opportunities for interhelical H-bonding, including interactions with glycine zipper motifs, and for ion and cofactor binding. Further, differences in wide turn subtype usage by related protein family members, such as the G-protein coupled receptors, rhodopsin and the  $\beta_2$ -adrenergic receptor, can significantly impact the orientation and position of residues critical for ligand binding and receptor activation.

MOL#43042

Over 70% of helices in proteins are curved or contain one or more kinks or other non- $\alpha$ -helical structures (e.g.  $\pi$ -bulges,  $3_{10}$ -helices, kinks) (Barlow & Thornton, 1988; Bansal, et al., 2000). This is particularly the case for polytopic transmembrane proteins, such as G-protein-coupled receptors and ion channels whose relatively long transmembrane helices – straight, curved or kinked – pack into compact elliptical or circular domains to form ligand binding pockets, or channels for the passage of ions. These non-canonical structures or deviations in  $\alpha$ -helicity, which are due to the perturbing effects of both prolyl and non-prolyl residues, identified here as the *signature* residue, are contained within one to two turns of a helix. They change the pitch of the helix and displace backbone atoms of involved residues from the positions they would normally occupy in an  $\alpha$ -helical structure. Using methods that reveal details about the shape of the helix, we previously identified three types of non-canonical structures: wide turns, tight turns and kinks. Specifically, we showed that non-canonical structures could be discerned from  $C_{\alpha_i} \rightarrow C_{\alpha_x}$  distance-difference plots, that is, plots of the differences between the  $C_{\alpha_i} \rightarrow C_{\alpha_x}$  distances ( $x = -2 \rightarrow -5$ ) of residues forming the non-canonical regions, and those of a regular  $\alpha$ -helix (Riek et al., 2001).

These  $C_{\alpha_i} \rightarrow C_{\alpha_x}$  distance-difference plots reveal alterations in regular  $\alpha$ -helical geometry because, although peptide bond lengths are essentially invariant and the distance between  $C_{\alpha}$  atoms of adjacent residues remains constant, rotations about the bonds on either side of the  $C_{\alpha}$  atom of each residue produce changes in the  $\phi$  and  $\psi$  dihedral angles, leading to altered distances between  $C_{\alpha}$  atoms two or more residues apart. As a result, non- $\alpha$ -helical regions are evident as positive or negative deviations in the distances between  $C_{\alpha}$  atoms two to five residues apart in sequence, compared with the equivalent residues in an  $\alpha$ -helix (Riek et al., 2001; Rigoutsos et al., 2003), (Supplemental Data, Fig. 1).

Although  $C_{\alpha_i} \rightarrow C_{\alpha_x}$  distance-difference plots allow wide turns, tight turns and kinks to be identified, neither such plots nor other analyses of helical architecture provide sufficient detail to fully characterize non-canonical regions. For example, Sugeta & Miyazawa (1967) and others (Aqvist, 1986; Christopher et al., 1996; Bansal, et al., 2000; Visiers, 2000; Visiers, 2001; Cordes et al., 2002; Bright and Sansom, 2003; Mohapatra et al., 2004; Lopera et al., 2005) determined the

MOL#43042

helical axis, the bend angle of the helix, the rise per residue and the inter-residue angle, by "best-fitting" the helical regions to a canonical four residue  $\alpha$ -helical template, using a centroid calculation (involving four consecutive  $C\alpha$  atoms), or a least-squares procedure, which involves one to two turns of helix either side of the bend created by a non-canonical segment, to calculate the bend angle. These approaches suffer from an inability to evaluate helical geometry on a residue-to-residue basis. Moreover, non-canonical segments, such as wide turns, involve an eccentric enlargement of the helical diameter resulting in lateral displacement of the helical axis. This behavior is not accurately modeled using available methods, which rather, artefactually skew and twist the helical axis. Other approaches to identify helical perturbations that result in wide turns, also called  $\pi$ -bulges, require the presence of one or more  $\pi$  ( $i \rightarrow i-5$ ) hydrogen-bonds (H-bonds) (Kabasch and Sander, 1983; Richards and Kundrot, 1988; Frishman and Argos, 1995; Labesse et al., 1997; Weaver, 2000; Fodje and Al-Karadaghi, 2002) and a turn of  $\alpha$ -helix before and after the wide turn (Cartailler and Luecke, 2004). As a result, wide turns not bounded by complete  $\alpha$ -helical turns may not be identified.

As we show here, these shortcomings can be obviated by calculating the change in helical direction on a residue-to-residue basis. This allows the effects of the signature residue and other residues within a non-canonical region, to be accurately determined. Using this approach, we have identified three distinct wide turn types in transmembrane protein helices - unique architectural features that provide opportunities for hydrogen-bonding interactions with adjacent helices, or for ion or cofactor binding.

## Methods

### Database and identification of helices

Transmembrane helical regions were identified using Insight II (Accelrys, San Diego, CA, USA). To determine potential H-bonding interactions typical of a  $3_{10}$ - ( $i \rightarrow i-3$ ),  $\alpha$ - ( $i \rightarrow i-4$ ) or  $\pi$ -helix ( $i \rightarrow i-5$ ), hydrogen atoms were added either at pH 7.0 or at the pH specified in the structure file.

MOL#43042

We treated the same proteins from different species as separate examples, if they display sequence differences in the non-canonical structures. Some proteins are highly represented with multiple entries in the database, particularly structures for photosynthetic reaction centers and bacteriorhodopsin. Initially we considered all such entries if the resolution criteria were met (resolution  $\leq 3.0\text{\AA}$  and an R-value  $\leq 0.3$ ). However, if the structures of the transmembrane helices were identical in the various entries, only one representative member was evaluated. In instances where structural variations were evident between entries for the same protein due to differences in crystallization conditions, to the different mutant forms, or different functional states, e.g., oxidized or reduced, or to crystallization in the presence or absence of different inhibitors or different metal ions, all such entries were considered in evaluating the detailed geometry of wide turns.

### Identification of non-canonical regions

Non-canonical segments were identified based on  $C_{\alpha_i} \rightarrow C_{\alpha_x}$  distance-difference plots (Supplemental Data, Table 1), as previously described (Riek et al., 2001). Here we focus on the wide turn or  $\pi$ -bulge category of non-canonical structures, which display  $C_{\alpha_{i-2}}$  and  $C_{\alpha_{i-3}}$  distance-differences that are positive, and  $C_{\alpha_{i-4}}$  and  $C_{\alpha_{i-5}}$  distance-differences that are negative.

In non-canonical helical regions with proline as the helix-perturbing residue, the position containing the proline is designated as the signature residue position ( $S_0$ ). Non-prolyl residues that disrupt  $\alpha$ -helical geometry result in similar  $C_{\alpha_i} \rightarrow C_{\alpha_x}$  distance-difference profiles to those produced by prolyl residues (Supplemental Data, Fig. 1D-F). In such instances, these non-prolyl residues are the signature residues. Thus, such non-prolyl residues are defined as the signature residue if their substitution by a proline would produce a similar  $C_{\alpha_i} \rightarrow C_{\alpha_x}$  profile.

### Helical parameters

The effects of the residues within a non-canonical region on helical structure can be seen from changes in the position and direction of the helical axis. To accurately determine such changes, we characterized transmembrane protein helices on a residue-to-residue basis. This was done by evaluating helical parameters that are based on the coordinates of the atoms forming

MOL#43042

each  $C_{\alpha_i} \rightarrow C_{\alpha_{i+1}}$  segment. From these coordinates, nine parameters could be determined: the three backbone dihedral angles,  $\phi$ ,  $\psi$  and  $\omega$ , the three bond lengths and the three bond angles of the backbone atoms. These parameters alone allow a helical segment of as little as four residues to be constructed. The regularity of such a four-residue helix enables other helical parameters to be calculated, including the helical spoke angle, the radius of the helical segment and the direction and length (rise per residue) of the helical axis (Riek et al., 2001). Based on these considerations, to determine the helical axis for any residue-to-residue pair, we constructed a *de novo* computed four-residue helix using the parameters determined from the particular  $C_{\alpha_i} \rightarrow C_{\alpha_{i+1}}$  segment being examined (Supplemental Data, Fig. 2). The regularity of such *de novo* constructed helices enabled precise trigonometrical determination of the positions of two helical axis points for each four-residue helix. The helical axis vector, which is equivalent to the rise per residue for each  $C_{\alpha_i} \rightarrow C_{\alpha_{i+1}}$  segment within the helical region of interest (Supplemental Data, Fig. 2C), was determined from the helical axis points. The vector of the helical axis indicates the helical path of a segment and is defined in terms of its direction, position and length.

The helical bend angle is the change in helical direction resulting from the effect of the signature residue on helical structure. This was determined by calculating the angle between the axis vectors of the  $S_0$ - $S_1$  and  $S_7$ - $S_6$  segments. The  $S_0$ - $S_1$  segment (designated as the reference segment with the signature residue at  $S_0$ ) was selected as it indicates the direction of the helix immediately C-terminal to the signature residue. In addition, given that the  $S_1$  residue is beyond the signature residue, the  $S_1$  side chain does not influence the helical structure of the segment. The  $S_7$ - $S_6$  segment was selected as it is the closest N-terminal segment to the non-canonical region that still has an  $\alpha$ -helical structure. With few exceptions, these segments are suitable indicators of the change in helical direction across all classes of non-canonical structure: wide turns, tight turns and kinks.

To assess the potential for backbone H-bond formation, the orientation of the C=O bond with respect to the helical axis was determined. For each segment in a wide turn region, the angle between the C=O bond and the helical axis was calculated. A backbone H-bond could form if the distance between the amide hydrogen atom donor and the carbonyl oxygen atom acceptor was

MOL#43042

$\leq 3.0\text{\AA}$  and the C-H $\cdots$ O and H $\cdots$ O=C angles were  $\geq 110^\circ$  and  $\geq 90^\circ$  (c.f. ref. Desiraju and Steiner, 1999), respectively.

### Detailed characterization of wide turns

With a regular  $\alpha$ -helix, the C $\beta$  atom of the side chain is directed towards the N-terminus. To examine how and where the effects of the pyrrolidine ring of proline or the side chain of other signature residues starts to affect helical structure in a non-canonical region, we chose to examine regions of the transmembrane helix extending from three positions C-terminal to eight positions N-terminal of the signature residue. This length of helix completely spans all non-canonical segments and, in addition, allows the steric effects of the pyrrolidine ring or other side chains that influence residues N-terminal to a non-canonical element, to be characterized. Including residues beyond either end of wide turn regions enabled parameters arising from coordinates spanning three or four residues, for example, inter-residue dihedral angles to be shown for the entire non-canonical region. Plots of the different parameters of these extended segments, therefore, include for comparison the capping helical structures at both ends of the perturbed region, and such plots reveal if an  $\alpha$ -helical segment or another non-canonical segment is part of a region being investigated.

To orient non-canonical regions for comparison of structural features, the helical axis point for the signature residue at position  $i$  was placed at coordinates 0,0,0 and then the helical axis vector rotated to lie along the positive x-axis (Supplemental Data, Fig. 3). Having fixed the orientation of the helical axis vector (defined by the helical axis points for residues  $i$  and  $i+1$ ), the entire helical region was then rotated to allow the C $\alpha_i$  atom to lie on the z-axis, that is at coordinate 0,0,z, where z is equal to the radius of the segment from  $i$  to  $i+1$ ; this orientation was designated as the 'standard' orientation.

## Results and Discussion

Over 3,000 individual transmembrane helical regions from 244 crystal structures deposited



MOL#43042

in the PDB (Berman et al., 2000) up to August 2007, were examined. The dataset was restricted to crystal structures with resolution  $\leq 3.0\text{\AA}$  and an R-value  $\leq 0.3$ . This set comprised 31 different proteins, including multichain protein complexes, with 350 transmembrane helices containing 70 wide turns. Although there is some uncertainty in the atom positions of structures with a resolution  $>2.2\text{\AA}$  but  $<3.0\text{\AA}$ , we included such structures, since, as noted by Engelman and colleagues (Senes et al., 2001), extended helical structures have an inbuilt degree of self-correction as the backbone atom positions have a greater degree of accuracy. NMR structures were considered but, with the exception detailed below, were not included because the structures determined do not necessarily represent the lowest energy state of all segments of transmembrane helices. As a result, deviations in C=O and N-H bond orientations may limit the formation of potential backbone H-bonds.

### Identification and classification of wide turn subclasses

Wide turns are characterized by the widening of a turn of a helix N-terminal to the signature residue or by the unwinding and lateral displacement of a two to three residue section of a helix (Fig. 1). As a result, the widened helix contains  $\sim 4.4$  residues per turn compared to 3.6 for an  $\alpha$ -helix. This is evident, for example, in the H chain of the photosynthetic reaction centers of *Rhodobacter sphaeroides* and *Thermophilus tepidum*, each with a single  $\alpha$ -helical transmembrane-spanning region. Alignment of these regions with the analogous region in the evolutionarily related organism, *Blastochloris viridis*, reveals the insertion of a single leucine residue (Leu30) in this transmembrane region, which in contrast to the *R. sphaeroides* and *T. tepidum* structures, is a helix that now contains a wide turn (Fig. 2A). The opposite may also be the case, that is, deletion of a residue in an evolutionarily conserved transmembrane segment results in the switch from a wide turn to an  $\alpha$ -helix (Fig. 2B).

To define wide turn regions in transmembrane segments, we used  $C\alpha_{i-1} \rightarrow C\alpha_x$  distance-difference profiles, since they are distinctive for such non-canonical structures and can readily discriminate between these and other non-canonical elements (tight turns or kinks) (Supplemental Data, Fig. 1). However, it was evident from such profiles that the width of the  $C\alpha_{i-4}$  and  $C\alpha_{i-5}$  traces

MOL#43042

varied (Fig. 3), and that these variations were directly related to the number of potential  $\pi$  H-bonds that could be formed N-terminal to the signature residue, S. Thus, although differences in the width of the  $C_{\alpha_{i-4}}$  and  $C_{\alpha_{i-5}}$  traces identified potential subclasses of wide turns, since the difference in the number of potential  $\pi$  H-bonds formed is a discrete variable, this was used as the basis for subclassifying them into three distinct subclasses as follows:  $W_1$ : one  $\pi$  H-bond between  $S_{-1}$  and  $S_6$  (Fig. 3A and E);  $W_2$ : two  $\pi$  H-bonds between  $S_{-1}$  and  $S_6$ , and  $S_{-2}$  and  $S_7$  (Fig. 3B and F), and  $W_3$ : three or more  $\pi$  H-bonds including those between residues at positions  $S_{-1}$  and  $S_6$ ,  $S_{-2}$  and  $S_7$ , and  $S_{-3}$  and  $S_8$  (Fig. 3C and G), (Table 1). The additional  $\pi$  H-bonds formed with the  $W_2$  and  $W_3$  wide turns involve interactions with residues N-terminal to the signature residue (Fig. 3D). Non-proline-induced wide turns have the potential to form an additional  $\pi$  H-bond between the amide hydrogen atom of the signature residue and the carbonyl oxygen atom of the residue at position  $S_{-5}$ . In such cases, the subclassification continues to be that based on the number of  $\pi$  H-bonds formed from the  $S_{-1}$  position. The distribution of proline- and non-proline-induced wide turns of each class is shown in Table 2.

As shown in Table 3, the range of  $\phi$  and  $\psi$  values at the  $S_{-5}$  to  $S_{-3}$  positions for the different wide turn subclasses overlap and cannot be used to distinguish between them. Similarly, as noted by Fodje and Al-Karadaghi (c.f. Figure 2a, (Fodje and Al-Karadaghi, 2002)), although a number of points lie outside the "preferred" region in the Ramachandran  $\phi$ - $\psi$  plot (Lovell et al., 2003) for the residues at the  $\pi_5$  position, (equivalent to the  $S_{-3}$  position in our study), a comparable number lie within the "preferred" region. Indeed, analysis of the  $\phi/\psi$  dihedral angles lead us to use the term "wide turn" instead of " $\pi$ -bulge", given that if the individual pairs of averaged  $\phi$  and  $\psi$  dihedral angles determined for the  $S_{-5}$  to  $S_{-2}$  positions (Table 3) are used to construct regular helices, none form a  $\pi$ -helix (that is, a helix with 4.4 residues per turn and  $i \rightarrow i-5$  H-bonding). In fact, the different  $\phi$  and  $\psi$  combinations for the  $S_{-3}$  position all produce either a left-handed helix or a circular helical path with a rise per residue of  $\sim 0\text{\AA}$  - a structural impossibility. Similarly, the  $\phi$  and  $\psi$  values for position  $\pi_5$  ( $S_{-3}$ ) (Table III of Fodje and Al-Karadaghi, 2002) also produce a circular structure. Most of these structures cannot form because of severe steric clashes between atoms on the adjacent

MOL#43042

turns. In addition, no  $\phi$  and  $\psi$  angle combinations yield a helix with  $\pi$  H-bonding as the major H-bond type. Although a  $\pi$ -bulge appears to mimic a segment of  $\pi$ -helix, the backbone dihedral angles indicate that it forms a structure with less than perfect  $\pi$ -helical character. Thus,  $\phi$  and  $\psi$  dihedral angles, *per se*, can neither be used to characterize wide turns nor to discriminate between different non-canonical types.

In several instances of wide turns, the number of  $\pi$  H-bonds indicated by H-bonding diagrams is fewer than the number expected based on the subclass indicated by the  $C_{\alpha_i} \rightarrow C_{\alpha_x}$  distance-difference profile. One such example is the wide turn induced by Pro215 in helix 5 of bovine rhodopsin (PDB: 1U19). This has a  $C_{\alpha_i} \rightarrow C_{\alpha_x}$  distance-difference profile typical of the  $W_3$  subclass (Fig. 4A) but the H-bonding diagram indicates only two rather than three  $\pi$  H-bonds (Fig. 4B). This is due to the combination of a  $\psi$  angle at position 211 that is less negative ( $53^\circ$  vs  $-40^\circ$ ) than for an  $\alpha$ -helix and a  $\phi$  angle that is more negative ( $-180^\circ$  vs  $-65^\circ$ ) at position 212. This forces the His211 C=O bond to deviate from its normal direction by  $75^\circ$  (Fig. 4C). This marked deviation of the 211 C=O bond is associated with a coincident reorientation of the H-N bond at position 212, which positions its hydrogen atom below the  $110^\circ$  cutoff angle (H-N $\cdots$ O) required for the formation of an  $S_{-3} \rightarrow S_{-8}$   $\pi$  H-bond. It is clear from a consideration of such aberrant wide turns that they could well be missed if their identification was based merely on the number of  $\pi$  H-bonds. In contrast, our method of detecting wide turns based on  $C_\alpha$  positions, which are the least likely to be perturbed even with wide turns that show the most marked structural deviation from that of an  $\alpha$ -helix, is much more robust.

In addition to the aberrant wide turn examples considered above that show very marked deviations in the C=O bond away from the helical axis, as noted by Fodje and Al-Karadaghi (2002) and Cartailier and Leucke (2004), almost all wide turns result in some degree of C=O bond deviation and, therefore, might be unable to form hydrogen bonds with amide hydrogen atoms in the adjacent C-terminal turn. With few exceptions, all proline-induced wide turns cause a deflection of the  $S_{-4}$  (and in some instances the  $S_{-5}$ ) C=O peptide bond by more (up to an additional  $60^\circ$ ) than the  $\sim 18^\circ$  observed in an  $\alpha$ -helix. This prevents a steric clash with the  $C\delta$  methylene moiety of the

MOL#43042

pyrrolidine ring and allows the amide hydrogen atoms of the residues on either side of proline to be located within H-bonding distance of the carbonyl oxygen atoms on the widened turn. The more negative the dihedral angles of the residue at position  $S_{-3}$  and the greater the difference between the  $S_{-3}$   $\phi$  and  $S_{-4}$   $\psi$  dihedral angles, the greater the deviation of the peptide bond plane with respect to the helical axis. However, the larger deviations do not always prevent a  $\pi$  H-bond from forming.

### **Influence of wide turn subclasses on helical architecture**

Residues in the vicinity of wide turn signature residues can also have a modifying effect on helical structure. To evaluate such effects, we examined non-canonical regions on a residue-to-residue basis. To this end, we determined the changes in direction of the helical axis vector at each position (Fig. 5), and examined the effects on the different wide turns arising from sequence and rotamer differences. By comparing the differences in direction (helical bend angle) and position between the reference axis vector and the vector for the  $S_{-7}$ - $S_{-6}$  segment (the last  $\alpha$ -helical segment before the beginning of a non-canonical region), it is possible to quantitate the different wide turns (Fig. 5). When the helical axis vectors determined between adjacent N,  $C_{\alpha}$  or C groups of atoms of the peptide backbone are displayed concurrently, the effect of each backbone dihedral angle on helical structure and direction is revealed (Fig. 5A, E and F).

Analysis of the helical bend angles shows differences between wide turn subclasses but also within subclasses. Except for the  $W_3$  subclass, proline-induced wide turns show greater bend angles, and a narrower range of bend angles, than do the wide turns induced by non-proline amino acids (Table 4). With the diversity of side chain structure for the non-proline amino acids, the wider range in bend angles is not unexpected. Although the signature residue, particularly if proline, is the major disruptive influence on the integrity of  $\alpha$ -helical structure, residues within the wide turn region also have an effect on the direction of the helix. This is seen with the shifts in position and direction of the axis vectors for the intermediate segments when compared with the reference segment vector (Fig. 5E and F). These shifts indicate that the change in helical direction is not limited to a single point on the helix but is the result of cumulative changes occurring over a number of segments. Fig. 5A-C show the paths of the N-terminal helical segments of a proline-

MOL#43042

induced wide turn of each subclass and the extent of the shift in helical axis. It is evident from Fig. 5 that the  $W_1$  subclass produces the largest shift in the helical axis in the region immediately N-terminal to the helical perturbation. The path traced by the axis vectors shows that for proline-induced wide turns, the backbone loops around the pyrrolidine ring and then bends away from the proline.

With proline-induced wide turns, the pyrrolidine ring and the formation of a single  $\pi$  H-bond act as the equivalent of inserting a 'wedge' into the helix, forcing it to bend away from the side containing the proline. With each additional  $\pi$  H-bond formed in the  $W_2$  and  $W_3$  wide turns, another 'wedge' is inserted into the helix but at an orientation equivalent to the position of the additional  $\pi$  H-bond. The effect or 'shape' of the wedge will be dependent upon the effects of the residues within the wide turn. Given that  $W_3$  wide turns have three or more  $\pi$  H-bonds, the combined effect can offset the effect of each individual  $\pi$  H-bond, resulting in negligible change in helical direction.

Aromatic,  $\beta$ -branched and large volume residues predominant in the eight positions N-terminal to the signature residue in proline-induced wide turns, whereas glycine, alanine, serine and threonine are usually found at two or more positions within this region in wide turns with a non-proline-residue at the signature position.  $W_3$  wide turns have a greater proportion of large volume residues compared with the  $W_1$  and  $W_2$  subclasses. Examples from a wider range of transmembrane protein families are needed before residue patterns characterizing each subgroup can be determined. Although wide turns are found throughout the transmembrane region, the majority of available examples lie towards the C-terminal region. However, there were a number of N-terminal region wide turns that were not included in the survey as they were either incomplete, in that they occurred in the last turn of the helix where the partial wide turn transitioned into coil-like or other non-helical geometries before the wide turn was completed, or the remaining N-terminal portion of the helix was one turn or less in length.

Although structures solved by NMR do not provide consistent H-bonding patterns to allow confident delineation of wide turn subclasses, the  $C_{\alpha_j} \rightarrow C_{\alpha_x}$  distance-difference profiles can be used to study the structure of the helical transmembrane segments. Analysis of the NMR-derived

MOL#43042

structures of PufX (Tunncliffe et al., 2006), a single transmembrane-spanning protein organizing the photosynthetic reaction centre (RC)-light harvesting complex of *R. sphaeroides* revealed up to four regions displaying profiles with wide turn characteristics (Supplemental Data, Fig. 4). Calculation of the mean and standard deviations of the  $C_{\alpha_i} \rightarrow C_{\alpha_x}$  distance differences determined for these various NMR structures, at each position, revealed some segments that are relatively fixed and others where the helical architecture is flexible, varying between wide turn and almost  $\alpha$ -helical geometries, eg the segment encompassing residues 34 to 37 (Fig. 7). In a number of purple bacteria, the photosynthetic RC is surrounded by a ring of light-harvesting  $\alpha\beta$  polypeptide chains (LH1). The RC reduces a quinone ( $Q_B$ ) successively over a number of cycles, and when fully reduced it moves from the RC through the membrane to an adjacent cytochrome  $bc_1$  complex (Cogdell et al. 2006). In *R. sphaeroides* PufX is proposed to fulfill two functions: to enable the formation of a LH1-RC dimer, and to provide a gap in the LH1 ring to allow the delivery of  $Q_B$  to the  $bc_1$  complex. The glycine zipper motifs present in PufX would stabilize dimer formation. Thus, it seems reasonable to suppose that flexibility in the transmembrane region of PufX is required to provide an opening within the bilayer for  $Q_B$  to move within the membrane, while at the same time maintaining its contacts with the LH1-RC dimer complex.

### Rotamer involvement in proline and non-proline wide turns

Proline, unlike other residues with side chains that can rotate around the  $C_{\alpha}$ - $C_{\beta}$  bond, is restricted to a single rotamer conformation with limited flexibility provided only by ring isomerization between *exo* and *endo* forms. With non-proline residues, one or more rotamer conformations is found in both wide turns and  $\alpha$ -helices (Dunbrack and Cohen, 1997; Lovell et al., 2000). This flexibility allows a wide turn to change its position along a transmembrane helical segment provided that the signature residue is not a proline.

An example of such a switch in the position of a wide turn is seen in helix 10, subunit I of bovine cytochrome C oxidase (BCCO) (Tuskihara et al., 2003; Muramoto et al., 2007). In the reduced state, the wide turn has a  $W_2$  profile with Gly384 as the signature residue. In the oxidized form, however, a  $W_3$  wide turn is present with the signature residue position now at Phe387 (Fig.

MOL#43042

6). To allow this isomerization to a different signature residue, two residues within this region (Leu381 and Ser382) have had to change their rotamer conformations (Fig. 6). Moreover, the wide turn has introduced a region of flexibility that is not available with an  $\alpha$ -helical geometry, or with a tight turn or kink.

### Modifying effects of other residues

The effects of residues apart from the signature residue on helical direction are demonstrated by the structures of helix 5 of bacterial rhodopsins. Two such structures have a proline at the  $S_2$  position of  $W_1$  non-proline-induced wide turns (Fig. 8A). These  $S_2$  prolines not only alter the direction of the helix (Fig. 8A) but also cause its marked lateral displacement (Fig. 8B and C) in the region N-terminal to the prolines, to allow the bulky pyrrolidine rings to be accommodated. This mechanism of pyrrolidine ring-accommodation differs from that used by other non-canonical helices in which there is little lateral displacement of the helix. Rather, the helix in the immediate N-terminal region loops out to accommodate the pyrrolidine ring (Figs. 1A and 8A (orange ribbon)). Since the  $S_2$  prolines prevent the wide turn from being propagated more N-terminally, only a single  $S_1 \rightarrow S_6$   $\pi$  H-bond is formed.

Because glycyl residues lack a side chain, the preceding N-terminal portion of the helix can be oriented more closely to the glycine than it could for a residue with a sidechain. Additionally, the lack of a sidechain allows a greater depolarization of the  $C_\alpha$ - $H_{\alpha 1}$  and  $C_\alpha$ - $H_{\alpha 2}$  bonds allowing the  $H_{\alpha 1}$  and  $H_{\alpha 2}$  atoms to form stronger H-bonds,  $\sim$ -2kcal/mol (Vargas et al., 2000; Scheiner et al., 2001), relative to  $CH \cdots O$  H-bonds formed by H atoms not bound to the backbone  $C_\alpha$  atom ( $\sim$ -0.5kcal/mol (Desiraju and Steiner, 1999)). The  $H_{\alpha 1}$  atom of glycine forms an intrahelical H-bond with the carbonyl oxygen of the *i*-4th residue on the preceding turn. Evaluation of 18 wide turns with a glycine at position  $S_1$  shows that the  $S_5$  position is closer to the  $S_1$  position by 1.1Å to 1.7Å, as compared to wide turns with  $S_1$  residues other than glycine (Supplemental Data, Fig. 5). The presence of the glycine can change helical direction by  $\sim$ 5°.

### Structural effects of wide turn subclasses

MOL#43042

Wide turns alter the register of a face of a helical segment C-terminal to the turn, compared to the orientation of the face before the turn, and the extent of this shift differs between the subclasses. It is smallest for the  $W_1$  subclass ( $-45^\circ$ - $75^\circ$ ), intermediate for the  $W_2$  subclass ( $60^\circ$ - $90^\circ$ ) and largest for the  $W_3$  subclass ( $80^\circ$ - $120^\circ$ ). This provides flexibility in helical architecture, allowing interactions between residues on the transmembrane segment in question with those on an adjacent helix, and in particular, allows backbone-to-backbone interactions that would otherwise not be possible with a rigid  $\alpha$ -helical structure.

An example of two wide turns underlying such interhelical interactions is shown in Fig. 9. Here a number of CH $\cdots$ O type H-bonds (predominantly C $\alpha$ H $\cdots$ O) stabilize interactions between transmembrane helix 1 of the A chain of BCCO, involving a glycine zipper motif (GxxxGxxG) (Senes et al., 2004; Mackenzie et al., 1997; Russ and Engelman, 2000; Senes et al., 2000; Kim et al., 2005), G<sub>23</sub>AWAGMVG<sub>30</sub>, and helix 2, which is in an antiparallel orientation to helix 1 and contains two wide turns. Both wide turns belong to the  $W_3$  subclass and produce  $<5^\circ$  changes in helical direction. As is evident, the first wide turn of helix 2 orients the C=O bond of residue Phe68 such that it interacts via a CH $\cdots$ O H-bond with the H $\alpha$ 2 atom of Gly23 in helix 1. Similarly, the second wide turn orients the C=O bond of Gly76 in helix 2 such that it can interact via a CH $\cdots$ O H-bond with H $\alpha$ 2 of Gly16 in helix 1. These interactions would not be possible if helix 2 lacked these wide turns, since the C=O bonds of Phe68 and Gly76 would not be directed towards their respective H-bonding partner residues. Moreover, the widening of the helix at the positions of the two wide turns brings these residues to within H-bonding distance of the adjacent helix. Importantly, because Phe68 and Gly76 bond to glycine donors (Gly23 and Gly16), the C $\alpha$ H $\cdots$ O bonds thus formed are stronger than usual CH $\cdots$ O bonds (Desiraju and Steiner, 1999; Scheiner et al., 2001; Vargas et al., 2000). The lack of sidechains on these glycines also facilitates interhelical packing that sterically would not be possible if residues containing sidechains occupied these positions (Fig. 9). Finally, because wide turns permit backbone-to-backbone interactions, the interacting helices pack more closely than would be possible with interactions involving sidechain-to-backbone, or sidechain-to-sidechain bonding, since the number of contacts, electrostatic or van



MOL#43042

der Waals, that can form with these latter interactions, is likely to be less. Other examples of a glycine zipper motif stabilizing interhelical contacts have been reported (Senes et al., 2000), but to our knowledge this is the first example of a glycine zipper interacting with a wide turn.

In contrast to these  $W_3$ -mediated interhelical interactions, interhelical interactions involving helices with  $W_1$  and  $W_2$  wide turns do not involve glycylic residues but rather residues that have sidechains with conventional H-bond donor properties. Moreover, the larger helical bend angles of the  $W_1$  and  $W_2$  subclasses (Table 4) limit the contacts between adjacent helices to only one or two H-bonding interactions. Nonetheless, the stronger conventional N/O-H...O H-bond formed in these cases may be required, given the limitation to only one or two interhelical H-bond interactions. Typically, these H-bonds are backbone-to-sidechain interactions usually involving tryptophan ( $H_{\epsilon 1}$  atom), serine ( $H_{\gamma 1}$ ), or threonine ( $H_{\gamma 1}$ ). The larger helical bends of the  $W_1$  and  $W_2$  wide turns and the involvement of a residue with a sidechain for interaction, provide the flexibility required to allow the helix containing such turns, and an adjacent interacting helix, to be oriented in either a parallel or anti-parallel fashion.

With the  $W_3$  turns involving glycylic donors, although both the  $H_{\alpha 1}$  and  $H_{\alpha 2}$  atoms can form H-bonds, their H-bonding roles are distinct. The  $H_{\alpha 1}$  atom is involved in intra-helical H-bonding or interhelical H-bonding to a carbonyl oxygen on an adjacent helix that runs in a parallel orientation. In contrast, the  $H_{\alpha 2}$  atom can only form interhelical H-bonds with a backbone carbonyl on an adjacent helix if it runs in anti-parallel orientation. This orientation is required, since a parallel orientation precludes H-bonding because both the  $C_{\alpha}$ - $H_{\alpha 2}$  bond and the C=O bond are aligned in the same direction.

### **Binding of cofactors, ions and ligands**

Wide turns have previously been noted to provide binding site for cofactors and ions (Fodje and Al-Karadaghi, 2002; Cartailier and Luecke, 2004). Several interesting examples are also evident from our analyses. For example, a  $W_2$  non-proline-induced wide turn is evident in helix 10 of the A chain of BCCO that binds the cofactor, HEME-A. A  $W_2$  wide turn (signature residue Gly801) is also seen in the absence of  $Ca^{2+}$  in helix 7 of rabbit muscle  $Ca^{2+}$  ATPase. However, in

MOL#43042

the presence of  $\text{Ca}^{2+}$  the wide turn structure is disrupted because residues previously involved in forming it now utilize their carbonyls to form a  $\text{Ca}^{2+}$  binding pocket. Finally, a proline-induced  $W_2$  wide turn in helix 5 of bovine rhodopsin helps to correctly position residues that line the binding pocket for the  $\beta$ -ionone ring of retinal. Upon photoactivation and isomerization of the chromophore from 11-*cis* to all-*trans* retinal to form the LUMI rhodopsin photo-intermediate, the  $\beta$ -ionone ring is now oriented so that it can interact with the  $S_{-4}$  carbonyl oxygen of the wide turn (Nakamichi and Okada, 2006).

With the recent release of the structure for another member of the GPCR superfamily, the  $\beta_2$ -adrenergic receptor (AR) (Cherezov et al., 2007), we can now identify regions within the transmembrane helices that differ from those of rhodopsin. Although the transmembrane domains (TM) in the two structures have similar orientations, there are both similarities and differences in their wide turns, the latter potentially being important for receptor activation by their distinctive ligands – biogenic amines in the case of the  $\beta_2$ -AR and 11-*cis* retinal in the case of rhodopsin. These include a wide turn in TM II of both receptors that in both instances is of the  $W_2$  subtype, and one in TM V that is of the  $W_3$  subtype in rhodopsin, but is a  $W_2$  wide turn in the  $\beta_2$ -AR. The  $\beta_2$ -AR also has a  $W_1$  wide turn induced by Pro168 in TM IV, with the carbonyl bond of Thr164 at the  $S_{-4}$  position of this wide turn being directed towards Ser203 on TM V. Although Thr164 and Ser203 are too widely separated to form an H-bond, it is of interest that Ser203 is critically involved in ligand binding, via a H-bond interaction with the *m*-hydroxyl of the catechol ring, as well as in receptor activation (Strader et al., 1989, Liapakis et al., 2000). Thus, Thr164 in the  $\beta_2$ -AR may be important for positioning the ligand to allow interaction between Ser203 and its *m*-hydroxyl. Rhodopsin has a proline-induced kink rather than a wide turn at the equivalent region in TM IV that, in contrast to the  $\beta_2$ -AR, orients the carbonyl bond of Ala168 (the residue equivalent to Thr164 in the  $\beta_2$ -AR) away from TM V (Suppl. Fig. 6).

In terms of the  $W_2$  versus  $W_3$  wide turn difference in TM V of rhodopsin and the  $\beta_2$ -AR, this changes the shape of the transmembrane domain containing these non-canonical regions to alter the positioning and orientation of residues N-terminal to the signature residue, including not only

MOL#43042

Ser 203 at the S<sub>8</sub> position, but Ser207 at the S<sub>4</sub> position. Like Ser203, Ser207 is also involved in ligand binding (in this instance via an H-bond interaction with the catechol ring *p*-hydroxyl) and in receptor activation (Strader et al., 1989, Liapakis et al., 2000). Thus, in the absence of a crystal structure for the  $\beta_2$ -AR, it is evident that modeling its binding pocket based on the rhodopsins crystal structure would mal-position this critical pair of serine residues, even if the same rotamer positions were maintained as those for Met207 and His211 - the rhodopsin TM V residues equivalent to Ser203 and Ser207 in the  $\beta_2$ -AR, respectively.

## Conclusion

Using methods to characterize non-canonical regions in transmembrane helices on a residue-to-residue basis, we have identified three different classes of wide turns based on C $\alpha_i$ →C $\alpha_x$  distance difference-profiles and the number and position of potential  $\pi$  H-bonds. We also show that wide turns result from a series of discrete changes over a number of residues, equivalent to either the widening of a turn or an unwinding of the helix. The path of the helical axis vectors indicates that for proline-induced wide turns, the helix bends around the proline instead of away from the proline, as occurs with tight turns and kinks. The structure of the wide turn introduces flexibility in the helix, which affords unique opportunities for interactions with adjacent helices. With the tools developed, we can more accurately define helical structure and determine the effect of side chain rotamer conformations, thus bringing us closer to being able to predict with greater accuracy, secondary and, to some degree, even tertiary structure, from primary sequence.

MOL#43042

## Acknowledgments

We are most grateful to Drs. Merridee Wouters, Siiri Iismaa and Daniela Stock for reading the manuscript and for critical input.

MOL#43042

## References

- Aqvist J (1986) A simple way to calculate the axis of an  $\alpha$ -helix. *Computers & Chemistry* **10**:97-99.
- Bansal M, Kumar S, and Velavan R (2000) HELANAL: A program to characterize helix geometry in proteins. *J Biomolecular Struct & Dynam* **17**:811-819.
- Barlow DJ, and Thornton JM (1988) Helix geometry in proteins. *J Mol Biol* **201**:601-619.
- Berman HM, Westbrook J, Feng Z, Gilliland G, Bhat TN, Weissig H, Shindyalov IN, and Bourne PE (2000) The Protein Data Bank. *Nucleic Acids Res* **28**:235-242.
- Bright JN, and Sansom MSP (2003) The flexing/twirling helix: exploring the flexibility about molecular hinges formed by proline and glycine motifs in transmembrane helices. *J Phys Chem B* **107**:627-636.
- Cartailler J-P, and Luecke H (2004) Structural and functional characterization of  $\pi$ -bulges and other short intrahelical deformations. *Structure* **12**:133-144.
- Cherezov V, Rosenbaum DM, Hanson MA, Rasmussen SG, Thian FS, Kobilka TS, Choi HJ, Kuhn P, Weis WI, Kobilka BK, and Stevens RC (2007) High-resolution crystal structure of an engineered human beta-2 G protein-coupled receptor. *Science* **318**:1258-1265.
- Christopher JA, Swanson R, and Baldwin TO (1996) Algorithms for finding the axis of a helix: fast rotational and parametric least-squares methods. *Computers & Chemistry* **20**:339-345.
- Cogdell RJ, Gall A, and Kohler J (2006) The architecture and function of the light-harvesting apparatus of purple bacteria: from single molecules to *in vivo* membranes. *Q Rev Biophys*

MOL#43042

**339**:227-234.

Cordes FS, Bright JN, and Sansom MSP (2002) Proline-induced distortions of transmembrane helices. *J Mol Biol* **323**:951-960.

Desiraju G, and Steiner T (1999) *The Weak Hydrogen Bond in Structural Chemistry and Biology*, chap. 2, Oxford University Press, Oxford.

Dunbrack RL, and Cohen FE (1997) Bayesian statistical analysis of protein sidechain rotamer preferences. *Protein Sci* **6**:1661-1681.

Fodje MN, and Al-Karadaghi S (2002) Occurrence, conformational features and amino acid propensities for the pi-helix. *Protein Eng* **15**:353-358.

Frishman D, and Argos P (1995) Knowledge-based protein secondary structure assignment. *Proteins* **23**:566-579.

Kabsch W, and Sander C (1983) Dictionary of protein secondary structure: pattern recognition of hydrogen-bonded and geometrical features. *Biopolymers* **22**:2577-2637.

Kim S, Jeon T-J, Oberai A, Yang D, Schmidt JJ, and Bowie JU (2005) Transmembrane glycine zippers: Physiological and pathological roles in membrane proteins. *Proc Nat Acad Sci USA* **102**:14278-14283.

Labesse G, Colloc'h N, Pothier J, and Mornon JP (1997) P-SEA: a new efficient assignment of secondary structure from C alpha trace of proteins. *Comput Appl Biosci* **13**:291-295.

Liapakis G, Ballesteros JA, Papachristou S, Chan WC, Chen X, Javitch JA (2000) The forgotten

MOL#43042

serines. A critical role for Ser-203<sup>5,42</sup> in ligand binding to and activation of the  $\beta$ 2-adrenergic receptor. *J Biol Chem* **275**:37779-37788.

Lopera JA, Sturgis JN, and Duneau J-P (2005) Ptuba: a tool for the visualization of helix surfaces in proteins. *J Mol Graphic & Mod* **23**:305-315.

Lovell SC, Word JM, Richardson JS, and Richardson DC (2000) The penultimate rotamer library. *Proteins* **40**:389-408.

Lovell SC, Davis IW, Arendall WB 3rd, de Bakker PI, Word JM, Prisant MG, Richardson JS, and Richardson DC (2003) Structure validation by C $\alpha$  geometry:  $\phi$ ,  $\psi$  and C $\beta$  deviation. *Proteins* **50**:437-450.

MacKenzie KR, Prestegard JH, and Engelman DM (1997) A transmembrane helix dimer: structure and implications. *Science* **276**:131-133.

Mohapatra PK, Khamari A, and Raval MK (2004) A method for structural analysis of  $\alpha$ -helices of membrane proteins. *J Mol Model* **10**:393-398.

Muramoto K, Hirata K, Shinzawa-Itoh K, Yoko-O S, Yamashita E, Aoyama H, Tsukihara T, and Yoshikawa S (2007) A histidine residue acting as a controlling site for dioxygen reduction and proton pumping by cytochrome c oxidase. *Proc Nat Acad Sci USA* **104**:7881-7886.

Nakamichi H, and Okada T (2006) Local peptide movement in the photoreaction intermediate of rhodopsin. *Proc Nat Acad Sci USA* **103**:12729-12734.

Richards FM, and Kundrot CE (1988) Identification of structural motifs from protein coordinate data: secondary structure and first-level supersecondary structure. *Proteins* **3**:71-84.

MOL#43042

Riek RP, Rigoutsos I, Novotny J, and Graham RM (2001) Non- $\alpha$ -helical elements modulate polytopic membrane protein architecture. *J Mol Biol* **306**:349-362.

Rigoutsos I, Riek P, Graham RM, and Novotny J (2003) Structural details (kinks and non-alpha conformations) in transmembrane helices are intrahelically determined and can be predicted by sequence pattern descriptors. *Nucleic Acids Res* **31**:4625-4631.

Russ WP, and Engelman DM (2000) The GxxxG motif: a framework for transmembrane helix-helix association. *J Mol Biol* **296**:911-919.

Scheiner S, Kat T, and Gu Y (2001) Strength of the C $\alpha$ -H...O hydrogen bond of amino acid residues. *J Biol Chem* **276**:9832-9837.

Senes A, Gerstein M, and Engelman DM (2000) Statistical analysis of amino acid patterns in transmembrane helices: the GxxxG motif occurs frequently and in association with beta-branched residues at neighboring positions. *J Mol Biol* **296**:921-936.

Senes A, Ubarretxena-Belandia I, and Engelman DM (2001) The C $\alpha$ -H...O hydrogen bond: A determinant of stability and specificity in transmembrane helix interactions. *Proc Nat Acad Sci USA* **98**:9056-9061.

Senes A, Engel DE, and DeGrado WF (2004) Folding of helical membrane proteins: the role of polar, GxxxG-like and proline motifs. *Curr Opin Struct Biol* **14**:465-479.

Strader CD, Candelore MR, Hill WS, Sigal IS, and Dixon RA (1989) Identification of two serine residues involved in agonist activation of the beta-adrenergic receptor. *J Biol Chem* **264**:13572-13578.



MOL#43042

Sugeta H, and Miyazawa T (1967) General method for calculating helical parameters of polymer chains from bond lengths, bond angles and internal-rotation angles. *Biopolymers* **5**:673-679.

Tsukihara T, Shimokata K, Katayama Y, Shimada H, Muramoto K, Aoyama H, Mochizuki M, Shinzawa-Itoh K, Yamashita E, Yao M, Ishimura Y, and Yoshikawa S (2003) The low-spin heme of cytochrome c oxidase as the driving element of the proton-pumping process. *Proc Nat Acad Sci USA* **100**:15304-15309.

Tunncliffe RB, Ratcliffe EC, Hunter CN, and Williamson MP (2006) The solution structure of the PufX polypeptide from *Rhodobacter sphaeroides*. *FEBS Lett* **580**:6967-6971.

Vargas R, Garza J, Dixon DA, and Hay BP (2000) How strong is the C<sup>α</sup>-H...O=C hydrogen bond? *J Am Chem Soc* **122**:4750-4755.

Visiers I, Braunheim BB, and Weinstein H (2000) Prokink: a protocol for numerical evaluation of helix distortions by proline. *Protein Engineering* **13**:603-606.

Weaver TM (2000) The pi-helix translates structure into function. *Protein Sci* **9**:201-206.

MOL#43042

## Footnotes

Supported in part by a grant (#354400) from the National Health and Medical Research Council, Australia.

MOL#43042

## Figure Legends

**Fig. 1.** Ribbon traces showing paths of wide turns and an  $\alpha$ -helix. (A) An  $\alpha$ -helix and  $W_3$  wide turn induced by prolines viewed along the helical axis from C- to N-terminus. This wide turn example has a  $<5^\circ$  change in direction. a, position at which the widened turn of the helix starts and then resumes  $\alpha$ -helical geometry one full turn further N-terminal. The position of the pyrrolidine ring is indicated by asterisk. Green ribbon:  $\alpha$ -helix; orange ribbon: wide turn. (B) The yellow ribbon shows the path of a  $W_1$  wide turn looping out and around the pyrrolidine ring. The grey lines show the path of an  $\alpha$ -helix. The path of a wide turn formed by a partial unwinding of the helix is indicated by the cyan ribbon. (C) View of (B) rotated by  $90^\circ$  showing the divergent paths of these wide turns. (Grey ribbon not shown).

**Fig. 2.** Effect of an insertion or loss of a residue on the helical architecture of various transmembrane segments. (A) Insertion of a residue in an  $\alpha$ -helical region is associated with a wide turn non-canonical structure. This is shown with the transmembrane region of the H chain of *B. viridis* (*B. v.*). Alignment of this region with the corresponding transmembrane regions (both  $\alpha$ -helices) of *R. sphaeroides* (*R. s.*) and *T. tepidum*, (*T. t.*) shows the region containing Leu30 of *B. viridis* looping out as a widened turn (orange ribbon) before resuming as an  $\alpha$ -helical structure. (B) Loss of a residue within a wide turn is associated with an  $\alpha$ -helical structure. This is illustrated in the case of helix 2 in *E. coli* ubiquinol oxidase (*E.c.*), which is homologous to the A chain of bovine (*Bov.*) cytochrome c oxidase (BCCO). In helix 2 in BCCO, there are conserved prolines at two positions (Pro72 and Pro84) and a conserved asparagine (Asn80). Aligning the ubiquinol oxidase with the *Paracoccus denitrificans* (*P.d.*) or *R. sphaeroides* (*R.s.*) BCCOs, places the proline (Pro72) and asparagine (Asn80) residues (both inducing wide turns in the bovine) at comparable positions, with the N-terminal regions of the proline-induced wide turns all following a similar backbone path. However, the region between Pro117 and Asn124 of ubiquinol oxidase (equivalent to Pro72 and Asn80, respectively, of BCCO) is  $\alpha$ -helical (orange ribbon), lacking the second wide turn as seen in

MOL#43042

the other three structures. Key conserved residues are indicated by dots. Arrows indicate positions of the two conserved prolines.

**Fig. 3.**  $C_{\alpha_i} \rightarrow C_{\alpha_x}$  distance-difference profiles and H-bonding patterns for  $W_1$ ,  $W_2$  and  $W_3$  wide turns.

(A-C):  $C_{\alpha_i} \rightarrow C_{\alpha_x}$  distance-difference plots. Color code: Difference between the distance between the  $C_{\alpha}$  atom of any residue,  $n$ , in the non-canonical regions indicated and that of residues at 2 ( $n-2$ ), 3 ( $n-3$ ), 4 ( $n-4$ ), 5 ( $n-5$ ) positions N-terminal, and the comparable distances in an  $\alpha$ -helix, are indicated by the blue, green, red and yellow traces, respectively. (A)  $W_1$ : *E. coli* Acrb multidrug efflux pump, helix 6, signature residue: Pro490. (B)  $W_2$ : BCCO, G chain, helix 1, signature residue: Pro26. (C)  $W_3$ : BCCO, A chain, helix 2: signature residue: Pro72. (D) Plots in (A-C) combined to allow comparison of differences in profiles.  $W_1$  wide turn (—);  $W_2$  wide turn (— —);  $W_3$  wide turn (- - -). The colors of the flat rectangles on the X-axis correspond to the colors of the helical axis vector for each segment (see Figure 5). (E-G): H-bonding interactions in the proteins indicated in (A-C), respectively, determined as described in Riek et al. (2001). Blue rectangles represent the amide hydrogen of the residue indicated, red rectangles represent the carbonyl oxygen and pink rectangles denote prolyl residues. The amino acid sequences are indicated by the single letter code, and are offset (from top to bottom) by four residues in keeping with the formation of  $n$  to  $n-4$  H-bonds in an  $\alpha$ -helix. Numbers above and below indicate sequence numbers. H-bond type: solid line (vertical):  $i \rightarrow i-4$ ; dashed line (sloping from upper right to lower left):  $i \rightarrow i-5$ . Bond length (indicated by the numbers on the connecting lines) color code: brown:  $< 2.0 \text{ \AA}$ , red  $< 2.2 \text{ \AA}$ , orange:  $< 2.4 \text{ \AA}$ , orange yellow:  $< 2.5 \text{ \AA}$ , mustard yellow:  $< 2.6 \text{ \AA}$ , green:  $< 2.7 \text{ \AA}$ , blue:  $< 2.8 \text{ \AA}$ , cyan:  $< 3.0 \text{ \AA}$ . (H) Different helical paths of the above  $W_1$ ,  $W_2$  and  $W_3$  wide turns. The segments have been aligned such that the signature residues at position  $S_0$  are coincident.

**Fig. 4.** A  $W_3$  wide turn with fewer than predicted  $\pi$  H-bonds. (A) The  $C_{\alpha_i} \rightarrow C_{\alpha_x}$  distance-difference plot of a non-canonical region spanning Met207 to Leu216 in helix 5 of bovine rhodopsin indicates a  $W_3$  wide turn based on the width of the negative deflections (red and yellow traces). (B) H-

MOL#43042

bonding diagram indicating that the  $\pi$  H-bond between Met207:O and Phe212:HN does not form. The absent  $\pi$  H-bond between Met207:O and Phe212:HN is indicated by the grey dotted line. (C) Helical structure of the non-canonical region containing the wide turn induced by Pro215 shows the skewed orientation of the His211 C=O bond as a result of its  $\psi$  dihedral angle being markedly less negative (+53°) than that of an  $\alpha$ -helix (-40°). This also produces a coincident reorientation of the H-N bond at position 212, leading to the distance between Met207:O and Phe212:HN (4.1 Å) being too great to allow an H-bond to form. Additionally, the orientation of the Phe212 HN bond, directed towards the helical axis, results in an N-H...O angle of 60° - much less than the minimum 110° required for an H-bond.

**Fig. 5.** Position and direction of  $N_i \rightarrow N_{i+1}$ ,  $C\alpha_i \rightarrow C\alpha_{i+1}$  and  $C_i \rightarrow C_{i+1}$  helical axis vectors over the non-canonical region for proline-induced  $W_1$  (yellow)  $W_2$  (pink) and  $W_3$  (blue) wide turns. (Note: the axis vectors of an  $\alpha$ -helix would form a straight line). An example from each wide turn subclass was placed in the 'standard' orientation and combined to form a single display. The  $C\alpha_{S0} \rightarrow C\alpha_{S+1}$  reference segment vector and the preceding eight N-terminal  $C\alpha_i \rightarrow C\alpha_{i+1}$  vectors are shown along with the backbone N,  $C\alpha$  and C atoms. Examples:  $W_1$  subclass induced by Pro490 in helix 6 of *E. coli* Acrb multidrug efflux pump (yellow);  $W_2$  subclass induced by Pro26 in helix 1 of the G chain of BCCO (pink);  $W_3$  subclass induced by Pro72 in helix 2 of the A chain of BCCO (blue). (A) View along the Z axis. (B) View along the X axis. (C) View along the Y axis. The N,  $C\alpha$  and C backbone atoms indicate the path of the helix and show the backbone at the  $S_{-4}$  position looping out around the position (arrow) of the pyrrolidine ring (not shown). (D) A view similar to (B) with the backbone atoms removed, and the  $S_0$  position highlighted by a white circle. The extent of the change in the vectors is indicated by the lighter coloring of the  $S_{-8}$  vectors. The  $W_1$  wide turn shows the greatest change in helical direction, the  $W_2$  wide turn a smaller divergence, and the  $W_3$  minimal change in direction. (E,F) Helical axis vectors of the same non-canonical segments as in (A-D), but determined based on the N and C atoms. The orientations are the same as shown in (A) and (C) above with the N and C vectors in (E) labeled showing position N-terminal to  $S_0$ . The orientations

MOL#43042

of the  $N_i \rightarrow N_{i+1}$  and  $C_i \rightarrow C_{i+1}$  axis vectors are similar to the  $C_{\alpha_i} \rightarrow C_{\alpha_{i+1}}$  vectors with the exception of the  $C_{S-4} \rightarrow C_{S-3}$  and  $N_{S-3} \rightarrow N_{S-2}$  axis vectors, which show a reversed direction and indicate segments with a left-handed orientation. Color code:  $S_0$  or reference vector, light (C series) and dark red (N series);  $S_{-1}$ , orange;  $S_{-2}$ , yellow;  $S_{-3}$ , green;  $S_{-4}$ , cyan;  $S_{-5}$ , blue;  $S_{-6}$ , purple;  $S_{-7}$ , dark pink;  $S_{-8}$ , grey.

**Fig. 6.** Redox-dependent alteration in a wide turn from a  $W_2$  to  $W_3$  subclass. (A) Helical path of the oxidized (green) and reduced (orange) helix 10 (A chain of BCCO) showing  $W_3$  and  $W_2$  configurations, respectively, and associated with different rotameric conformations of Ser382. The different rotamers allow Ser382:Hy to act as an H-bond donor for binding to a pyrrole ring on heme A or to an OH moiety on the tail of heme A. (B,C) H-bonding diagrams (see Fig. 3 for details) of the helix in (A) with Phe387 as the signature residue in the oxidized form (B), and Gly384 as the signature residue in the reduced form (C) which has changed to  $\alpha$ -helical structure in the region N-terminal to Ala385 and Val386.

**Fig. 7.** Mean  $C_{\alpha_i} \rightarrow C_{\alpha_x}$  distance-differences (upper panel) and their standard deviations (histogram, lower panel) for the helical region of PufX. The mean  $C_{\alpha_i} \rightarrow C_{\alpha_x}$  distance-difference profiles show the presence of four regions with wide turn characteristics at Gly<sup>30</sup>, Gly<sup>35</sup>, Gly<sup>40</sup> and Phe<sup>47</sup> in the transmembrane segment (Trp<sup>22</sup>  $\rightarrow$  Gly<sup>52</sup>). As is evident from the standard deviation histograms, the wide turn at Phe<sup>47</sup> shows very little variation in  $C_{\alpha_i} \rightarrow C_{\alpha_x}$  distance-differences compared to the other three wide turns. Consistency of the Phe<sup>47</sup> wide turn structure is likely the result of hydrophobic/aromatic interactions between Trp<sup>33</sup> and Val<sup>37</sup> and between Phe<sup>38</sup> and Leu<sup>42</sup>. Color codes as indicated in Fig. 3.

**Fig. 8.** Modifying effects of non-signature residues on helical direction. (A) Differences in the helical axis vectors for  $W_1$  wide turn-containing helices with proline or leucine at the  $S_{-2}$  position and threonine or proline, respectively, at the signature residue position. Green: sensory rhodopsin II (SR2), helix 5; orange: *E. coli* Acrb multidrug efflux pump, helix 6. The effective size of the

MOL#43042

pyrrolidine rings is indicated by the green and orange balls. With proline at the  $S_0$  position, (orange), the N-terminal helical path moves out and around the ring with the helical path bending away. Proline at the  $S_{-2}$  position, (green), has the N-terminal path unwinding to place the ring beyond the helical path. (B) The extent of the displacement in (A) is shown by the 2.0Å lateral shift (SR2) in the axis vector (blue) of the  $S_{-5}$  segment N-terminal to the reference segment (red). By comparison, the lateral displacement of a proline-induced  $W_1$  wide turn lacking a prolyl residue at the  $S_{-2}$  position is only 1.1Å. (C) Comparison of the effects of a proline at the  $S_0$  and  $S_{-2}$  positions on helical structure. The SR2 helix above is shown in green. The  $W_1$  wide turn in helix 6 of the *E.coli* Acrb multidrug efflux pump is shown in orange, and the path of an  $\alpha$ -helix is shown in grey. The structures are aligned with the prolines superimposed and indicated by the blue ball.

**Fig. 9.** Multiple interhelical interactions made possible by the presence of wide turns and glycy residues in adjacent transmembrane helices. Multiple backbone-to-backbone C-H...O H-bonds (dashed lines) between helices 1 (orange) and 2 (green) of the A chain of BCCO are shown. Helix 1 contains a glycine (Gly23) that interacts with Phe68 located on a  $W_3$  wide turn in helix 2 induced by Pro72. Helix 1 also contains another glycine (Gly16) that interacts with both Gly76 and Gly77 located on another helix 2  $W_3$  wide turn induced by Asn80. In addition, backbone-to-sidechain interhelical H-bonds are evident between His12:O and Asn80:H $\beta$ 1 (2.3Å), Gly23:O and Met69:H $\gamma$ 2 (2.5Å), Pro72:O and Tyr19:H $\beta$ 1 (2.7Å) and Asn80:O and His12:H $\delta$ 1 (1.8Å). An additional sidechain-sidechain H-bond occurs between Thr17:O and Trp81:H $\epsilon$ 1 (2.2Å). The intrahelical H-bond, Gly76:O→Asn80:H $\beta$ 2 orients the Asn80 sidechain enabling the interhelical H-bond Asn80:O→His12:H $\delta$ 1 to form.

MOL#43042

**Table 1.** Wide turn helical conformations in transmembrane proteins

Sequences containing the wide turn region are listed with the signature residue indicated in bold. The protein chain designation followed by the transmembrane helix number and the signature residue (SR) position and amino acid type are indicated. The PDB accession number identifies the crystal structure of the protein containing the wide turn.

Sequence	Chain	SR	PDB	Sequence	Chain	SR	PDB
<b>W<sub>1</sub> subclass:</b>				<b>W<sub>2</sub> subclass :</b>			
<b>Proline</b>				<b>Proline</b>			
VLVALILTPALC	A6	490P	2J8S	IPVVCWLMPTVV	I1	23P	1JB0
YAIITYTIL <b>PK</b> QA	A6	252P	1XME	YSAHTFVLP <b>W</b> LI	A6	192P	1VF5
VVWAREYI <b>P</b> KIM	A11	473P	2A65	LFIFVIVR <b>P</b> PIE	A3	75P	2HYD
HAVHTYV <b>KP</b> FGD	A2	45P	2NWL				
<b>Non-proline</b>				<b>Non-proline</b>			
LDVSAKVG <b>F</b> GLI	A7	219F	1C3W	FYKFVA <b>V</b> AERKKK	I1	42K	2DYZ
LDVFAKYV <b>F</b> AFI	A7	245F	1E12	HFHYVLSM <b>G</b> AVF	A10	384G	2EIJ
LDLVTKVG <b>F</b> GFI	A7	208F	1H2S	FMVFGGFT <b>T</b> TLY	A2	93T	1U19
LPFFSKVG <b>F</b> SFL	A7	213F	1XIO	LWELVIEQ <b>F</b> EDL	A1	57F	1SU4
LDVTAKVG <b>F</b> GFV	A7	224F	1VGO	LFMTIPG <b>I</b> ALFY	A1	29A	1U7G
VYYLVG <b>P</b> MTEA	A5	146T	1H2S	YVLF <b>F</b> GFT <b>S</b> KAE	A5	158S	1QKO
LWGIWN <b>P</b> LRAKT	A5	151R	1XIO	GGISK <b>G</b> IER <b>F</b> AK	A5	193R	2A65
LYYLLT <b>S</b> LRSA	A5	162R	1VGO	LWVNLVTD <b>G</b> LPA	A7	801G	2AGV
LSALVTD <b>W</b> AASA	A5	184A	1E12	LYVIG <b>V</b> SCT <b>Y</b> DV	A7	235T	2CFQ
FLGFHS <b>F</b> G <b>L</b> YVH	A7	458L	1JB0	AGGT <b>V</b> VH <b>I</b> NAAI	A5	170N	2NS1
YLFTAIV <b>G</b> AMGW	B5	149A	1YEW	LQILL <b>V</b> Y <b>F</b> VLLK	A8	249V	2NWL
QKMAM <b>F</b> AG <b>G</b> ASG	C3	95G	1Q16				



**MOL#43042**

LLWWWYLGGAIVE	A2	163G	2IC8
LSWFFIFGGMIE	A2	78G	2NR9
GLWGVTMLKRLI	A9	303K	2NS1
AYVMAEQGVHVV	A7	222V	2NWL

**W<sub>2</sub> subclass :**

**Proline**

FLTFGLALPSVA	G1	26P	2DYS
LWLTFVYAPFAH	A4	131P	1U7G
VWLTLSYIPIAH	A4	142P	2B2H
FCVLQVFRPLLL	L3	136P	1VRN
YLTLVLFVRPVM	L3	136P	1AIJ
VLCIGCIHPTLV	M3	163P	1VRN
WMVLGFIRPILM	M3	165P	1AIJ
GLGNFLRFVQA	A1	32P	2A65
IAFLLVGIPLMW	A2	57P	2A65
YYVMRYITPAFL	A11	457P	2A65
NMFFFDIYPYIA	C1	13P	1Q16
LEAVLFLLPWSF	A5	210P	1XME
FAYFLIIVPVIS	C8	368P	1KB9
FLILVLMPTAG	C8	367P	1PPJ
GHQIHVSLPINK	A3	222P	1JB0
GHLIHVVAIPESZ	B3	199P	1JB0

**W<sub>3</sub> subclass :**

**Proline**

VMIFFMVMPIMI	A2	72P	2DYS
LMMFFVVIIPALF	A2	105P	1AR1
LMMFFVVIIPALF	A2	113P	2GSM
MFVVHFIIPLIV	A5	215P	1U19
IIEFYLSYPIYI	C4	182P	1YEW
PFFIFIFGPLLQ	A3	97P	2CFQ

**Non-proline**

PIMIGGFGNWLV	A2	80N	2DYS
PALFGGFNYFM	A2	113N	1AR1
PALFGGFNYFM	A2	121N	2GSM
YVLSMGAVFAIM	A10	387F	2DYS
YVMSLGAVFGIF	A10	422F	1AR1
NVIIGGVVFGCF	A10	430F	2GSM
HLAGLLGLGSLA	A3	208G	1JB0
HLAGLFGVSSLA	B3	185S	1JB0
GVLNAIVFTQLF	A2	81T	1XME
HLQVASLVTLTA	A10	394T	1XME
KAEVILGGSISI	A7	296S	2A65
DFWAGTIGVVFF	A10	412V	2A65
TVVLLYLRRDR	H1	34R	1VRN
YLVCFCFKQLA	A11	358K	2CFQ

MOL#43042

**Table 2:** Distribution of proline- and non-proline-induced wide turn subclasses

	$W_1$	$W_2$	$W_3$	$W_1 + W_2 + W_3$
Proline	4 (6%)	19 (27%)	6 (8%)	29 (41%)
Non-proline	16 (23%)	11 (16%)	14 (20%)	41 (59%)
Total	20 (29%)	30 (43%)	20 (28%)	70

MOL#43042

**Table 3:  $\phi$  and  $\psi$  dihedral angles  $\pm$ 1S.D. for the different subclasses of wide turns**

Proline-induced:

RP	$W_1$		$W_2$		$W_3$		$W_1 + W_2 + W_3$	
	$\phi$	$\psi$	$\phi$	$\psi$	$\phi$	$\psi$	$\phi$	$\psi$
-8	-68 $\pm$ 7	-36 $\pm$ 10	-68 $\pm$ 21	-49 $\pm$ 24	-53 $\pm$ 12	-48 $\pm$ 6	-65 $\pm$ 19	-47 $\pm$ 20
-7	-64 $\pm$ 6	-44 $\pm$ 8	-66 $\pm$ 6	-38 $\pm$ 8	-66 $\pm$ 11	-50 $\pm$ 9	-65 $\pm$ 7	-41 $\pm$ 10
-6	-65 $\pm$ 2	-43 $\pm$ 4	-62 $\pm$ 6	-48 $\pm$ 7	-72 $\pm$ 7	-43 $\pm$ 16	-64 $\pm$ 7	-46 $\pm$ 9
-5	-68 $\pm$ 3	-27 $\pm$ 11	-76 $\pm$ 18	-38 $\pm$ 7	-90 $\pm$ 23	-40 $\pm$ 12	-78 $\pm$ 19	-37 $\pm$ 10
-4	-91 $\pm$ 10	-30 $\pm$ 16	-92 $\pm$ 11	-22 $\pm$ 12	-107 $\pm$ 9	6 $\pm$ 15	-95 $\pm$ 12	-17 $\pm$ 18
-3	-114 $\pm$ 10	-20 $\pm$ 26	-121 $\pm$ 16	-54 $\pm$ 10	-132 $\pm$ 16	-62 $\pm$ 9	-122 $\pm$ 16	-51 $\pm$ 18
-2	-113 $\pm$ 25	-45 $\pm$ 4	-64 $\pm$ 12	-55 $\pm$ 7	-66 $\pm$ 6	-56 $\pm$ 8	-71 $\pm$ 22	-54 $\pm$ 8
-1	-59 $\pm$ 7	-39 $\pm$ 8	-58 $\pm$ 7	-49 $\pm$ 5	-58 $\pm$ 8	-50 $\pm$ 4	-58 $\pm$ 7	-48 $\pm$ 6
0	-57 $\pm$ 3	-37 $\pm$ 6	-59 $\pm$ 6	-41 $\pm$ 9	-55 $\pm$ 4	-47 $\pm$ 9	-58 $\pm$ 5	-42 $\pm$ 9
1	-68 $\pm$ 6	-38 $\pm$ 5	-67 $\pm$ 9	-39 $\pm$ 10	-59 $\pm$ 13	-49 $\pm$ 10	-65 $\pm$ 10	-41 $\pm$ 10
2	-71 $\pm$ 6	-29 $\pm$ 9	-57 $\pm$ 34	-41 $\pm$ 9	-69 $\pm$ 15	-53 $\pm$ 14	-62 $\pm$ 29	-42 $\pm$ 13
3	-79 $\pm$ 11	-36 $\pm$ 11	-62 $\pm$ 24	-31 $\pm$ 18	-69 $\pm$ 14	-48 $\pm$ 9	-66 $\pm$ 22	-35 $\pm$ 17

Non-proline-induced:

RP	$W_1$		$W_2$		$W_3$		$W_1 + W_2 + W_3$	
	$\phi$	$\psi$	$\phi$	$\psi$	$\phi$	$\psi$	$\phi$	$\psi$
-8	-60 $\pm$ 4	-44 $\pm$ 5	-66 $\pm$ 8 <sup>a</sup>	-41 $\pm$ 13 <sup>a</sup>	-65 $\pm$ 7	-42 $\pm$ 9	-63 $\pm$ 7	-42 $\pm$ 12
-7	-59 $\pm$ 5	-45 $\pm$ 7	-65 $\pm$ 6 <sup>a</sup>	-39 $\pm$ 8 <sup>a</sup>	-69 $\pm$ 8	-4 $\pm$ 414	-60 $\pm$ 29	-41 $\pm$ 17
-6	-62 $\pm$ 5	-44 $\pm$ 4	-65 $\pm$ 6	-35 $\pm$ 26	-79 $\pm$ 14	-52 $\pm$ 8	-68 $\pm$ 12	-44 $\pm$ 16
-5	-66 $\pm$ 6	-42 $\pm$ 12	-87 $\pm$ 23	-44 $\pm$ 14	-82 $\pm$ 6	-48 $\pm$ 18	-78 $\pm$ 16	-45 $\pm$ 15
-4	-73 $\pm$ 15	-21 $\pm$ 18	-79 $\pm$ 18	-32 $\pm$ 22 <sup>b</sup>	-80 $\pm$ 20	-27 $\pm$ 19	-79 $\pm$ 18	-22 $\pm$ 27
-3	-106 $\pm$ 21	-70 $\pm$ 14	-103 $\pm$ 26	-56 $\pm$ 20	-99 $\pm$ 18	-69 $\pm$ 13	-104 $\pm$ 20	-64 $\pm$ 20
-2	-69 $\pm$ 16	-44 $\pm$ 10	-62 $\pm$ 28	-53 $\pm$ 21	-60 $\pm$ 8	-47 $\pm$ 9	-65 $\pm$ 16	-49 $\pm$ 12
-1	-63 $\pm$ 5	-43 $\pm$ 7	-53 $\pm$ 23	-36 $\pm$ 15	-63 $\pm$ 6	-41 $\pm$ 11	-62 $\pm$ 9	-41 $\pm$ 10
0	-62 $\pm$ 7	-39 $\pm$ 22	-62 $\pm$ 8	-46 $\pm$ 7	-69 $\pm$ 10	-37 $\pm$ 11	-64 $\pm$ 9	-40 $\pm$ 16
1	-67 $\pm$ 24	-39 $\pm$ 10	-66 $\pm$ 7	-40 $\pm$ 6	-69 $\pm$ 10	-43 $\pm$ 13	-68 $\pm$ 16	-41 $\pm$ 11
2	-64 $\pm$ 5	-36 $\pm$ 29	-62 $\pm$ 6	-43 $\pm$ 9	-69 $\pm$ 11	-41 $\pm$ 11	-65 $\pm$ 8	-40 $\pm$ 20
3	-67 $\pm$ 19	-39 $\pm$ 8	-65 $\pm$ 8	-39 $\pm$ 10	-65 $\pm$ 13	-36 $\pm$ 20	-66 $\pm$ 15	-37 $\pm$ 14

MOL#43042

Combined:

RP	W <sub>1</sub>		W <sub>2</sub>		W <sub>3</sub>		W <sub>1</sub> + W <sub>2</sub> + W <sub>3</sub>	
	φ	ψ	φ	ψ	φ	ψ	φ	ψ
-8	-61± 6	-43± 7	-67±17	-45±23	-62±10	-44± 9	-64±13	-44±16
-7	-60± 5	-45± 7	-59±34	-36±17	-68± 9	-46±13	-62±23	-41±15
-6	-62± 4	-44± 4	-63± 6	-43±18	-76±13	-49±12	-67±10	-45±14
-5	-67± 6	-39±13	-81±20	-40±11	-84±14	-46±17	-78±17	-41±14
-4	-77±16	-23±18	-90±15	-20±28	-88±21	-17±23	-85±18	-20±24
-3	-108±20	-60±26	-116±18	-53±18	-109±23	-67±13	-112±20	-59±20
-2	-78±25	-44± 9	-64±17	-57±10	-62± 8	-50±10	-67±19	-51±11
-1	-62± 6	-42± 7	-58±11	-45± 9	-62± 7	-43±11	-60± 9	-44± 9
0	-61± 7	-38±20	-60± 7	-43± 9	-65±11	-40±11	-61± 8	-41±14
1	-67±21	-39±10	-67± 8	-39± 8	-66±12	-45±12	-67±14	-41±10
2	-65± 6	-35±27	-59±28	-42± 9	-69±12	-45±13	-64±20	-41±17
3	-70±19	-38± 9	-63±20	-33±16	-66±13	-39±18	-66±18	-36±15

RP, residue position. '0' marks the position of the signature residue. Negative values indicate positions N-terminal to the signature residue. Position 3 in the helix-C region in the results of Cartailier and Luecke (2004) is equivalent to the position of the signature residue. In the Fodje and Al-Karadaghi study (2002), position  $\square+1$  corresponds to the signature residue position.

<sup>a</sup> One point removed from each set because the positions were beyond the helical region (helix A5, 2NS1).

<sup>b</sup> One value removed because a *cis* peptide bond 25I-26P produces 25I  $\square$  angle of +100° skews the results if included.

MOL#43042

**Table 4:** Helix bend angles

	$W_1$	$W_2$	$W_3$
Proline	$40^\circ \pm 5^\circ$ <sup>a</sup>	$23^\circ \pm 7^\circ$	$14^\circ \pm 6^\circ$
Non-proline	$22^\circ \pm 7^\circ$	$14^\circ \pm 9^\circ$	$11^\circ \pm 7^\circ$

<sup>a</sup> Mean  $\pm$ 1S.D.

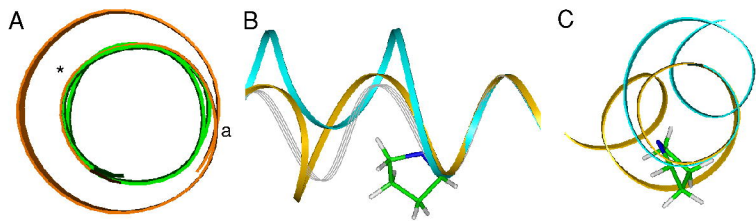
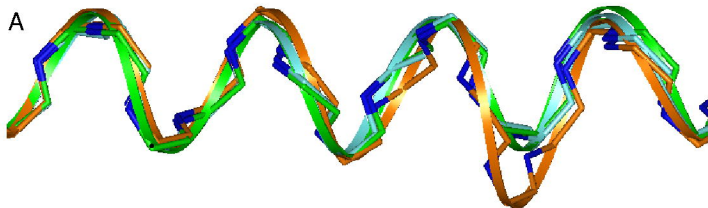
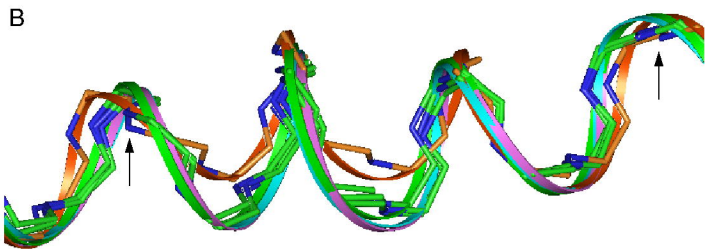


Fig. 1



<i>T. t.</i> :	13	QITIWAFWLF	FFFGLII	-YLRR	32
<i>R. s.</i> :	14	SLAIYSFWIF	LAGLIY	-YLQT	33
<i>B. v.</i> :	14	QLVWYAQWL	VIVT	VVLLYLRR	34



<i>Bov.</i> :	67	FFMVMPIMIG	GGFNWLVPLMI	87
<i>P. d.</i> :	100	FFVVIPALF	GGFGNYFMPLHI	120
<i>R. s.</i> :	108	FFVVIPALF	GGFGNYFMPLHI	128
<i>E. c.</i> :	112	FFVAMPFVI	-GLMNLVVPLQI	131

Fig. 2

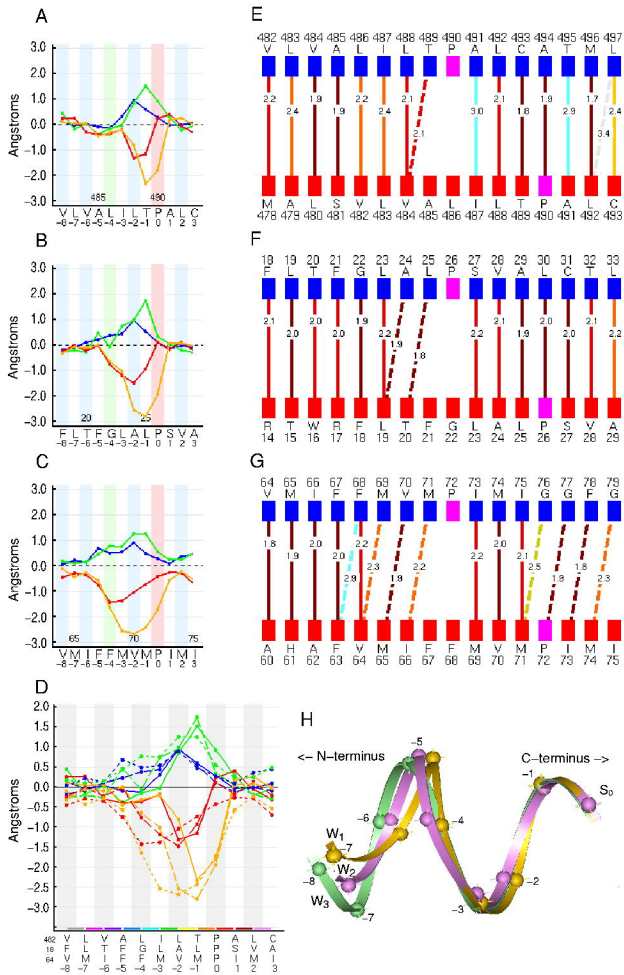


Fig. 3



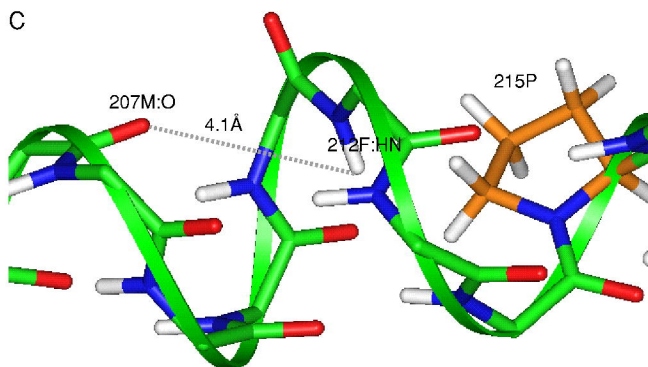
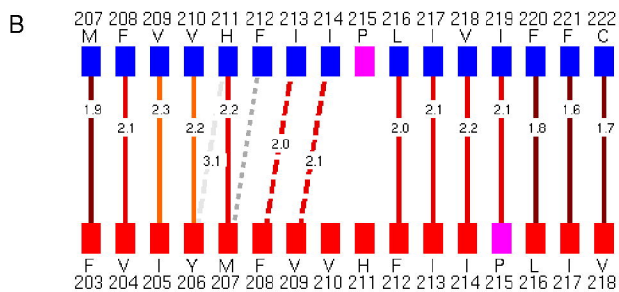
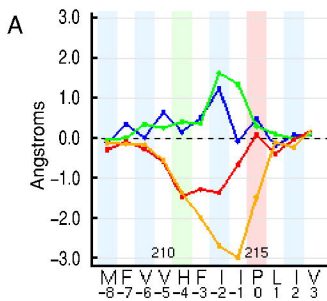


Figure 4

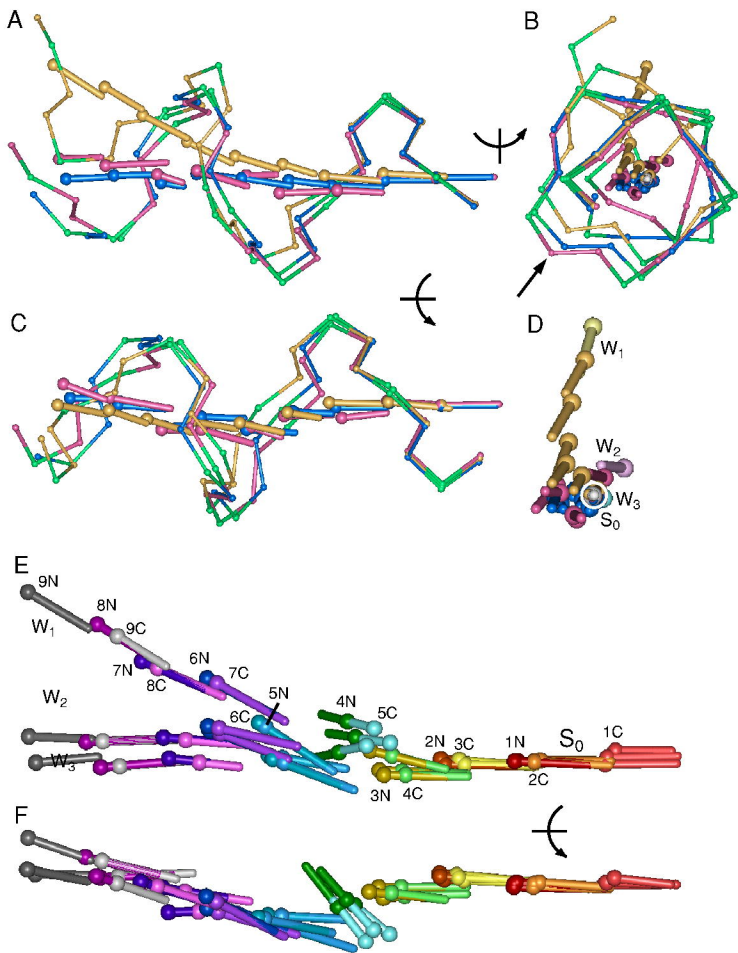


Fig. 5

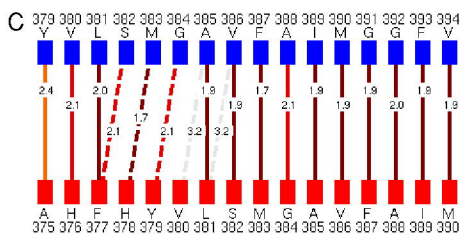
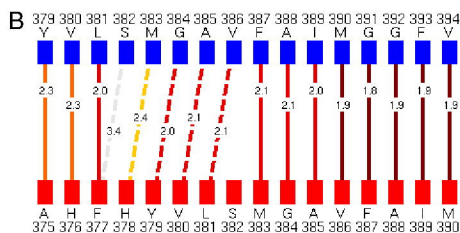
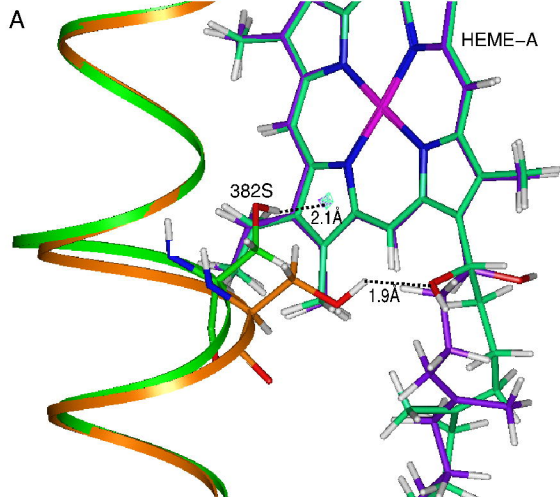


Fig. 6

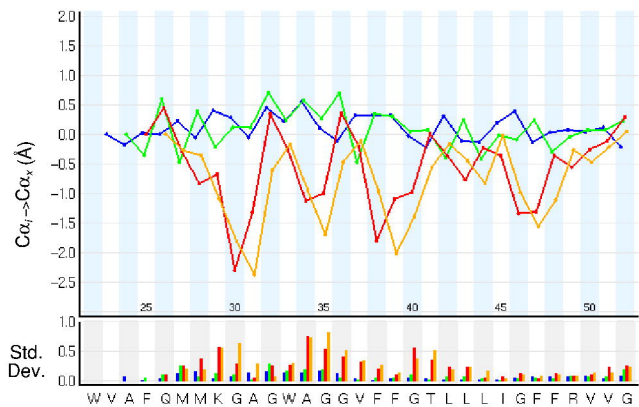


Fig. 7.

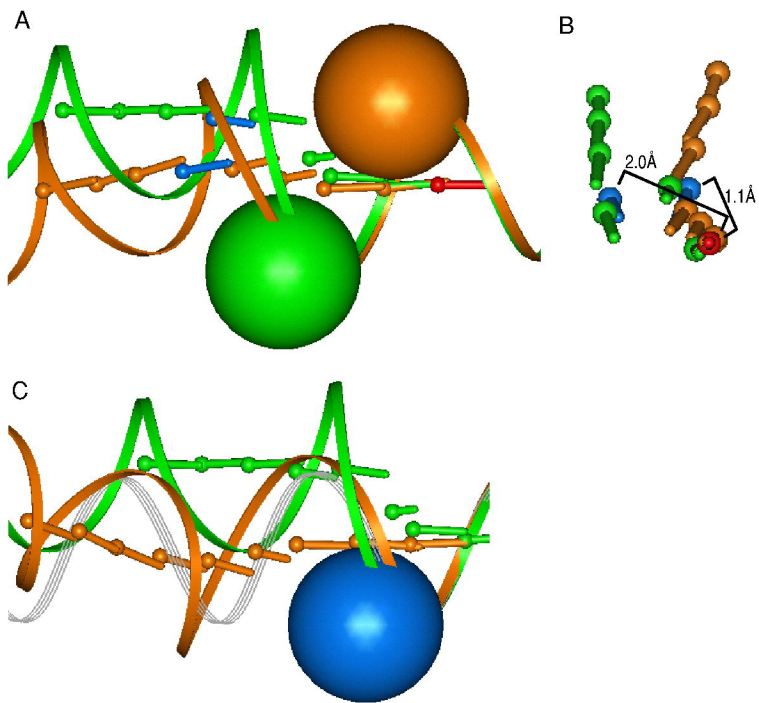


Fig. 8

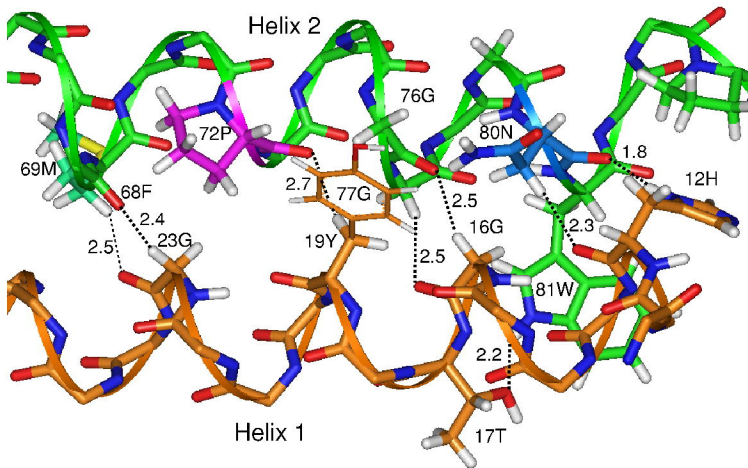


Fig. 9